H2020 MARIE SKŁODOWSKA-CURIE ACTIONS

Smart Mitigation of flow-induced Acoustic Radiation and Transmission for reduced Aircraft, surface traNSport, Workplaces and wind enERgy noise

Grant Agreement No 722401

D2.2 – Interim WP2 report

Acoustic Attenuation: Interim Public Report

Authors: N. Sayyad Khodashenas (KTH), M. D'Elia (CNRS/LAUM), T. Laurence (EPFL), C. Teruna (TUD), C. Sanghavi (SISW), H. Boden (KTH)

Due date: 31st December 2018

Table of Contents

1. Introduction

This report gives an interim summary of the work on noise attenuation techniques of SmartAnswer fellows:

ESR3, Niloofar Sayyad Khodashenas, KTH

ESR4, Massimo D'Elia, LAUM

ESR5, Thomas Laurence, EPFL

ESR7, Christopher Teruna, TUD

ESR14, Chaitanya Sanghavi, SISW

2. Effect of high level acoustic excitation and combinations of grazing/bias flow ("complex loads") on micro-perforate impedance (ESR3)

2.1. Introduction

Perforate plates and micro-perforated plates (MPP) are devices used to absorb sound and reducing its intensity. These materials appears in many technical applications, e.g. automotive mufflers, aircraft engine liners, combustion chambers, ventilation systems and room acoustics. Taking the air traffic development as an example travel both nationally and internationally has increased and although the aircrafts are becoming quieter the noise impact in the environment has not decreased. The propulsion system in an aircraft is the major source of noise especially during the take-off. Another example is the internal combustion engine in road vehicles which is important for the total noise at low speed e.g. inside cities. Perforates in the automotive mufflers are used to confine the mean flow, and reduce back-pressure but also for attenuation of sound. It is well known from the literature that the acoustic properties of perforates depend on the mean flow field, temperature, and the acoustic excitation level [2.1-2.4]. Therefore, different models and experimental techniques for characterization of Micro-perforated including flow and non-linearity are important.

There are large number papers on the effect of high-level acoustic excitation on the acoustic properties of perforates. It is well known form the literature that they can become non-linear at fairly low acoustic excitation levels. These non-linear losses are associated with practical velocity in the hole and vortex shedding at the outlet side of the perforated opening at high pressure levels. For pure tone excitation, the impedance will be associated with the acoustic particle velocity at that frequency. If the acoustic excitation is random or periodic with multiple harmonics the impedance at a certain frequency will depend on the particle velocity at other frequencies [2.5-2.8]. Studying this harmonic interaction with the purpose to increase the physical understanding and to develop a model including these effects is the main goal of this part of the project.

2.2. Impedance tube measurements for nonlinear samples

So far ESR3 has been making experimental studies on a 2.4% open area perforate plate using tonal and broadband excitation. The figure below shows a sketch of the experimental test rig. Work is ongoing to further improve the experiments and to analyze the data. The purpose of using broadband random excitation is to gain the ability to directly extract the nonlinear acoustic properties from a limited set of experimental data.

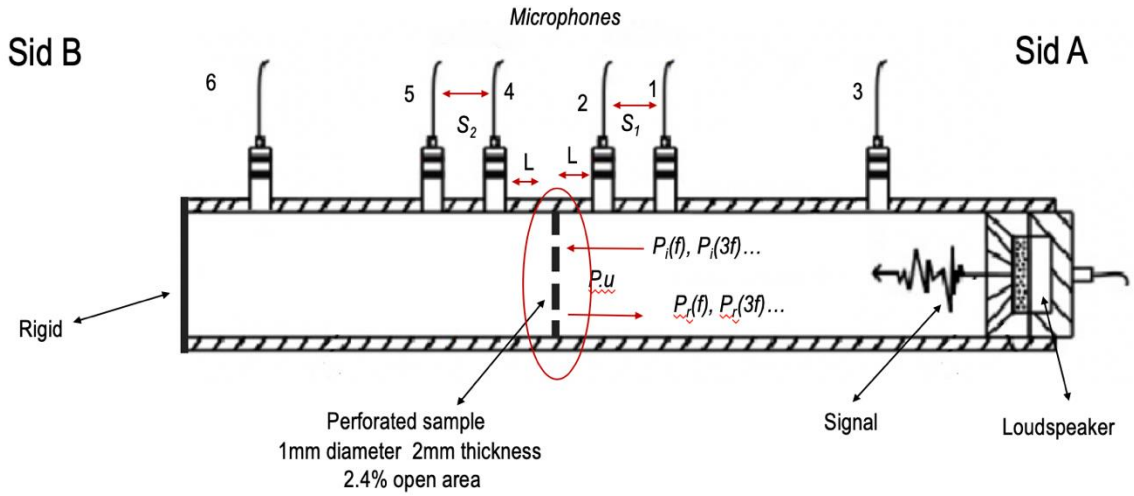

Figure 2.1. Schematic of the setup.

2.3. Techniques for determination of multi-port data

In [2.6] the nonlinear scattering matrix was suggested as a possible technique to study of harmonic interaction effects using tonal excitation. In order to determine the parameters of the nonlinear scattering matrix using only impedance tube data series of assumptions and simplifications need to be made following the discussion in [2.6].

- First it has been assumed that the signals are analytical.
- Second, the nonlinear energy transfer only occurs from lower frequency components to higher frequency harmonics.
- Third, the nonlinear energy transfer is only to odd harmonics.
- Finally, there is only one frequency component with high level excitation and the system components for other frequencies can be determined from linear scattering matrix or reflection coefficient measurements.

With these simplifying assumptions the nonlinear scattering matrix describingthe relation between the high-level excitation at frequency f and response at f and 3f can be described by the following matrix equation,

$$\begin{pmatrix} P_r(f) \\ P_r(3f) \end{pmatrix} = \begin{bmatrix} S_{f,f} & 0 \\ S_{3f,f} & S_{3f,3f} \end{bmatrix} \begin{pmatrix} P_i(f) \\ P_i(3f) \end{pmatrix} \quad (2.1)$$

The assumption of nonlinear energy transfer only from lower to higher harmonics gives $S_{f,3f}$=0, One further assumption made is that $S_{3f,3f}$ = R(3f) can be measured through a separate low-level excitation measurement at frequency 3f. The other component $S_{f,f}$ =R(f), is measured with varying level excitation at f, and it can be calculated form reflection coefficient at f Then the term caused by nonlinear energy transfer from the excitation frequency to the third harmonic , $S_{3f,f}$, can be determined.

2.4. **Preliminary results**

Nonlinear scattering matrix data for the impedance tube configuration was measured for different levels of excitation for both random and tonal ton excitation. Figure 2.2 shows the absolute value of $S_{3f,f}$ which is the scattering coefficient from an incident frequency to the third harmonic. It shows the result of taking the scattering matrix data from for 10 level of excitation for 5 different frequencies using single tone excitation.

2.5. **Conclusions and further work**

The method of determining nonlinear scattering matrix data from band-limited broadband random excitation instead of from single tone excitation was shown to be potentially promising in [2.9]. Comparisons will be made between the outcome of applying the nonlinear scattering matrix method to data both for tonal and band-limited random excitation. Conclusions will be drawn about the suitability of using broad-band excitation for these types of studies. If possible an empirical model describing the harmonic interaction in the form of a nonlinear scattering matrix will be suggested.

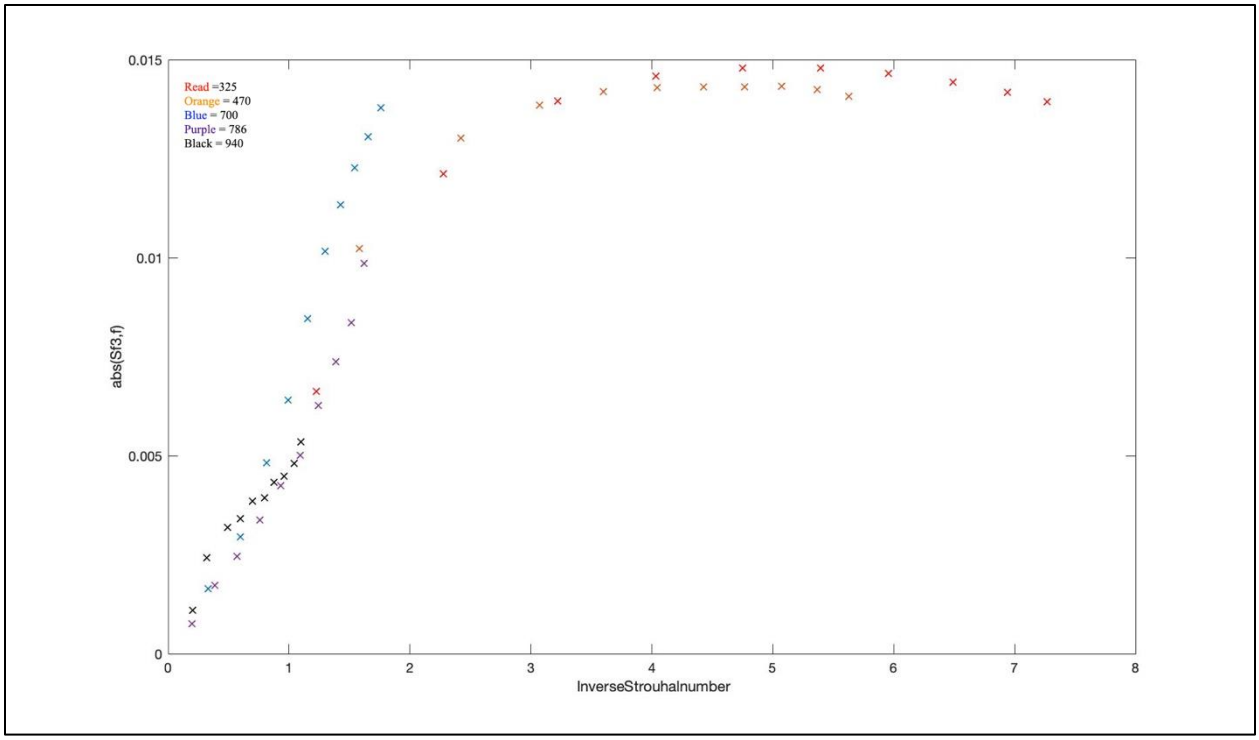

Figure 2.2. Absolute value of scattering matrix element $S_{3f,f}$ as a function of the inverse Strouhal number (Abs(u)/(wd) based on the particle velocity(u) and the hole diameter (d) for five different frequencies of excitation.

.

2.6. References

[2.1] Sivian, I.J. "Acoustic impedance of small orifices", Journal of the Acoustical Society of America 7 (1935) 94–101.

[2.2] Ingård, U.S. and Labate, "Acoustic circulation effects and the nonlinear impedance of orifices", Journal of the Acoustical Society of America 22 (1950), 211–219.

[2.3] Ingård, U.S. and Ising, H. "Acoustic nonlinearity of an orifice", Journal of the Acoustical Society of America 42 (1967) 6–17.

[2.4] Melling, T.H. "The acoustic impedance of perforates at medium and high sound pressure levels", Journal of Sound and Vibration 29 (1973) 1–65.

[2.5] Bodén, H., "Experimental investigation of harmonic interaction effects for perforates", AIAA Paper 2005- 2896.

[2.6] Bodén, H. "One-sided multi-port techniques for characterisation of in-duct samples with nonlinear acoustic properties", Journal of Sound and Vibration, Vol. 331, 2012, pp. 3050-3067.

[2.7] Bodén, H. "Two-sided multi-port techniques for characterisation of in- duct samples with non-linear acoustic properties." Acustica united with Acta Acustica, 99, 359-378, 2013.

[2.8] Bodén, H. Acoustic Characterisation of Perforates using Non-linear System Identification Techniques, AIAA-2007-3530, (2007).

[2.9]. Sayyad Khodashenas, N., Bodén, H. And Boij S. Determination of nonlinear acoustic properties of perforates using band-limited random excitation. Proceedings of EuroNoise 2018.

3. Aeroacoustics of meta-materials and MEMS (ESR4)

ESR 4 is focusing on the aeroacoustics behaviour of meta-materials and MEMs with attention brought not only to the flow effects on acoustics but also to the effects of acoustics on the flow.

The first investigated material has been a corrugated surface. The reasons behind such a choice are several: first of all, it is a widely used solution when there is both the requirement of strength and flexibility in industrial pipes. Then, as in our case, corrugations are particularly small, the acoustic field is expected to be linear (at given conditions) and somewhat close to what is expected to find in more complex metamaterials (where measurements will be, on the other hand, more complex). Therefore, the objective of the investigation is the acoustic-hydrodynamic interaction, particularly, the enhanced vorticity shedding due to the acoustic waves, which can often induce self-sustained oscillations and even failures in industrial applications. Finally, such investigations have not been carried out before for so small cavities (4 mm). In fact, other than evidently more restrictive space constraints, in this case the lower intensity of aeroacoustic interaction, and the generally higher frequencies, make measurements more troublesome.

The main effect of the aeroacoustic interaction is the enhancement of the transmission coefficient when compared with the same configuration but in a zero mean flow for Strouhal numbers of ~0.4. It can be seen, as shown in Figure 3.1, that for our configuration (i.e. 4 mm cavity and a Mach number ~0.07) the transmission coefficient is higher with flow than without at a signal frequency of 2 kHz. This is obviously due to the interaction between the acoustic signal and the shear flow produced by the presence of the cavities, which have been investigated by acoustic and optical techniques, as later described.

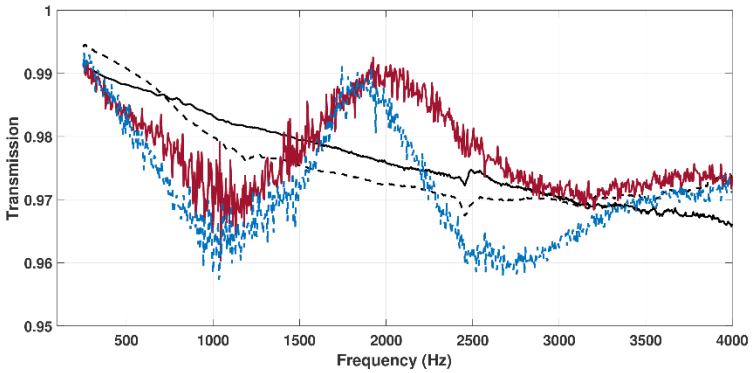

Figure 3.1 Absolute value of Transmission Coefficient. The solid and dash black lines represent the T+ and T- curves for the M = 0 case. The red and blue lines represent the T+ and T- curves for the M = 0.07 case, respectively.

Another subject of study was a classic microperforated liner composed by honeycomb Helmholtz resonators. In this case, the liner has been used as a test bench to compare the accuracy of numerical

multimodal methods by comparison with LDV experimental and K-method data. Very good coherence between the numerical method and LDV acoustic fields has been achieved (K-Method data is under retrieval). Also, the educed impedances are correlated with theoretical values. Therefore, further work will be carried out in obtaining more quantitative comparison among the three methods and in the analysis of the hard/soft wall interface.

Main interest was to investigate the interaction of a grazing flow with an incident acoustic signal. This has been done both by microphone measurements and optical techniques. The former can be used with an eduction method to obtain a global information of reflected and transmitted signals (usually by the means of a T-R technique) or local information about wavelength numbers' evolution along the test section (by the means of a K-method technique). Both techniques are available and have been used at LAUM to investigate a classic Helmholtz resonators liner and a corrugated surface. In the first case, two groups of four microphones are flush mounted before and after the test section in a symmetric fashion. By knowing the relative calibrations and positions, it is possible to link the scattering matrix of the system to the pressure measured by each microphone, which give an overdetermined set of measurements. In the second case, 11 microphones can be flush mounted inside the test section, opposite to the liner wall, in 22 positions (as their support has 2 positions). From these measurements it is possible to retrieve information about the acoustic field (i.e. acoustic wavenumbers) inside the test section.

Furthermore, the same elements have been investigated by the means of the Laser Doppler Velocimetry (LDV) technique. Here, two couples of laser beams intersect forming a fringe pattern: when a scattering particle passes through a Doppler signal is retrieved. Since this frequency is linked to the velocity of the particle, a velocity can be measured in two directions. With this technique, the spatial resolution is actually limited by the tray system which displaces the laser. In this case, a spatial resolution of 0.10 mm in a 2D plane can be obtained, as the 2D field approximation stands when measurements are made close to the centerline and in a symmetric configuration.

For the case of a corrugated surface, an experimental investigation by the means of microphones and LDV is carried out in order to give new insights in acoustic-hydrodynamic interaction. First of all, was important to verify that it was possible to identify frequency ranges where transmission coefficients are higher/lower than the corresponding no-flow configuration. This was done by microphone measurements, which allow the inspection of a broad range of frequencies in a single measurement. Then, LDV measurements have been carried out in an enhanced configuration of frequency and Mach number.
Results obtained up to today show that we were able to resolve the flow field in a very shallow corrugation by means of LDV with good accuracy: the shear layer can be correctly resolved and we can see how fluctuating velocity phase changes linearly through the cavity as shown in Figure 3.2.

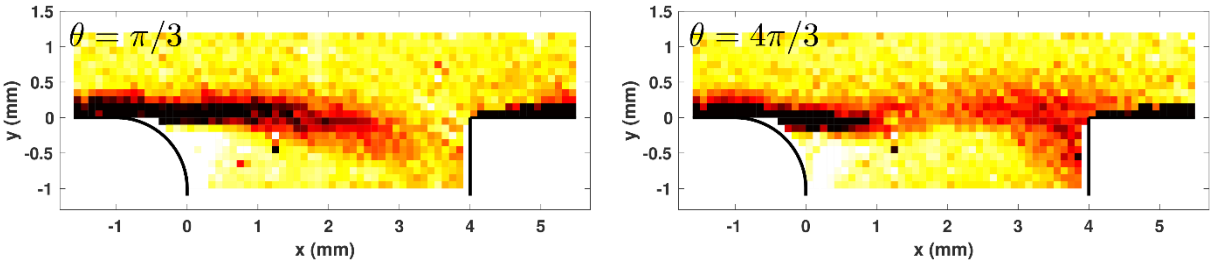

Figure 3.2 Measurements by Laser Doppler Velocimetry (LDV) of the total vorticity over a small cavity in a corrugated wall.

4. Locally and Non-Locally impedance controlled liners for noise transmission mitigation (ESR5)Introduction

The concept of Local Impedance Control, as well as Non-Local (or Distributed) Impedance Control, have been introduced in the Deliverable 3.1 “Low-Transmission: state-of-the-art and potential synthesis report”. These impedance control strategies are applied thanks to a programmable Digital Signal Processor, which controls the current inside the loudspeaker to vary its membrane velocity. The control output is based upon the measured acoustic pressure in the vicinity of the loudspeaker membrane. In this way a desired impedance behaviour could be reproduced.

The enforceability of a desired impedance then, as well as its effectiveness, essentially depends upon the complexity of the impedance law itself on the one hand, and on the other upon our knowledge of the electro-mechano-acoustical proper dynamics of the loudspeaker. Some preliminary experimental result will be given concerning the achievable acoustic performances and the stability concerns.

The desired impedance can be designed to maximize the absorption of the device, but this impedance can also be designed to achieve a specified behaviour of the wave reflected upon its surface. By arranging a liner in the form of an array of controlled loudspeakers, the transmission in an acoustic waveguide can be modified.

4.1. The Locally Controlled electroacoustic absorber

4.1.1. Single degree of freedom (SDOF) control

The SDOF local control law has been tested on a VISATON K50WP loudspeaker opportunely shunted with a digitally implemented control architecture, based on the averaged pressure of 4 microphone measurements on the 4 corners around the speaker.

The measured mobility is reported in Figure 4.1 for a target resistance equal to half the characteristic impedance of air, and for different values of the coefficients μ_1,μ_2 (look at 0, chapter 2.1 for the definition of these control parameters). The locally controlled loudspeaker mobility is compared to the Open Circuited loudspeaker mobility in **Error! Reference source not found.**. T he increase of the mobility peak and the widening of the frequency bandwidth, corresponds to higher acoustic performances in terms of normal absorption coefficient.

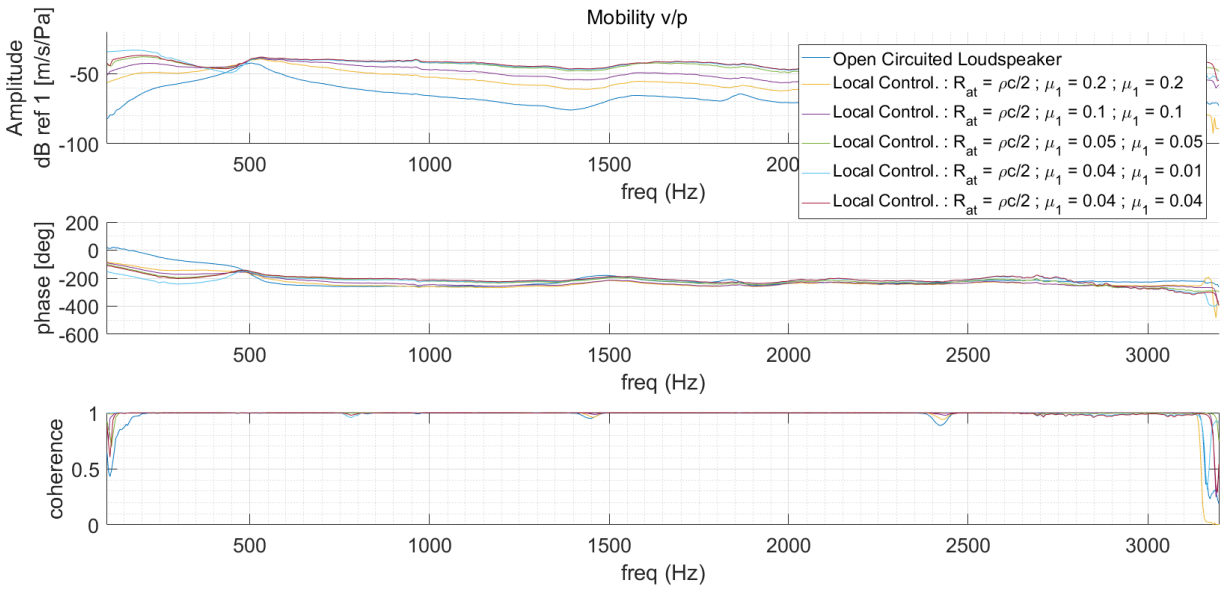

Figure 4.1: Measured mobility in Open Field, of a locally controlled loudspeaker.

Though, what we are mainly interested in here, is the acoustic transmission performances achieved by a liner made up of such electroacoustic resonators.

The Insertion Losses reported in Figure 4.2, are relative to a liner composed by a single controlled loudspeaker, placed on one side of a square section waveguide, of edge dimension equal to 5 cm. The loudspeaker membrane diameter approximately covers all the lateral side of the duct. Different values of the parameters involved into the Local Control are tested. By changing the target resistance R_{at} we can find the optimal value to get the maximum IL at resonance. It is possible to change the resonant frequency of the electroacoustic absorber as well, by varying the ratio μ_2/μ_1.

Lower values of the parameters μ_1 and μ_2 would allow a larger frequency bandwidth of efficient absorption and of IL consequently. The lowest values these parameters can achieve are nevertheless limited by stability issues, related to the acoustic feedback of the narrow sectional duct, and the inevitable time delay in the control.

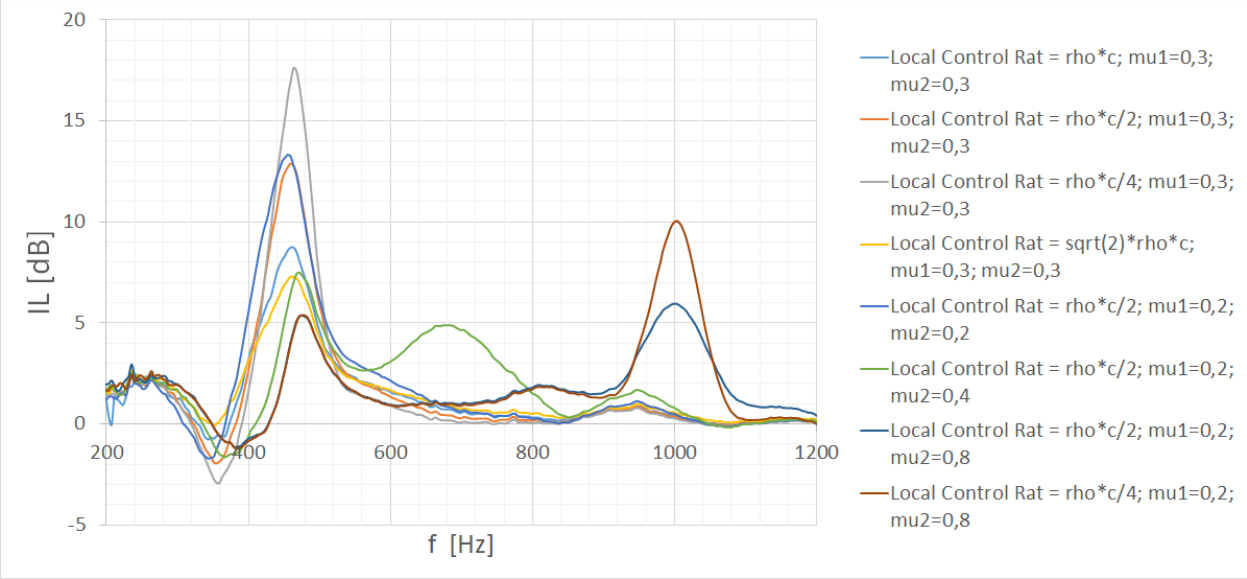

Figure 4.2: IL of a single-cell liner with different Local Control laws applied.

4.1.2. Multiple degrees of freedom control

Described in [4.5], the multiple degree of freedom approach to the controlled loudspeaker allows a different design of the target acoustic impedance, with several resonances, dispatched in frequency. Although it can be used to further improve the absorption performances of the loudspeaker, it can also be used in reflection control, with a different target. We will see in a next part how to design the interaction of an array of impedances to create insertion loss. The goal, on the loudspeaker scale, is to have a controlled phase of the reflection coefficient over a large frequency-band. Namely, the target phase ϕ is of the form $\phi = -a\ log(f) + b$ (**Error! Reference s ource not found.**), with f being the frequency. To be able to perform this phase, the control of the loudspeaker is set to a 3-DOF control, with a target impedance of the form:

$$Z = \sum_{1}^{3} \frac{1}{\frac{1}{Z_i}}, \qquad with\ Z_i = R_i + j\omega M_i + \frac{1}{j\omega C_i}.$$

Since the reflection coefficient and the impedance are directly linked, an optimization process targeting the phase function we introduced above, and taking as variables the nine parameters of the 3-DOF impedance can be run to know the impedance that has to be imposed to reach the target phase. The target impedance and its experimental realization via real-time control are shown on Figure . This demonstrates the possibility of designing an acoustic impedance suitable to reflection control.

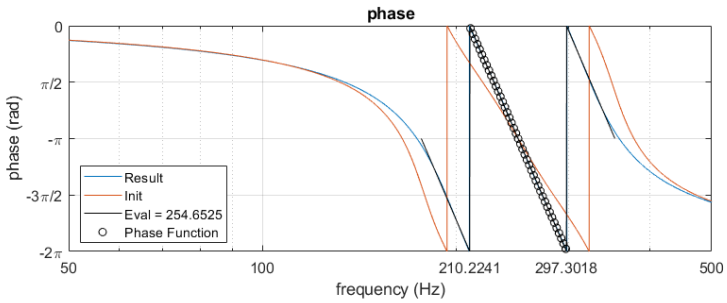

Figure 4.3: Phase target (in black), initial state (orange) and final state (blue) of the optimization process**.**

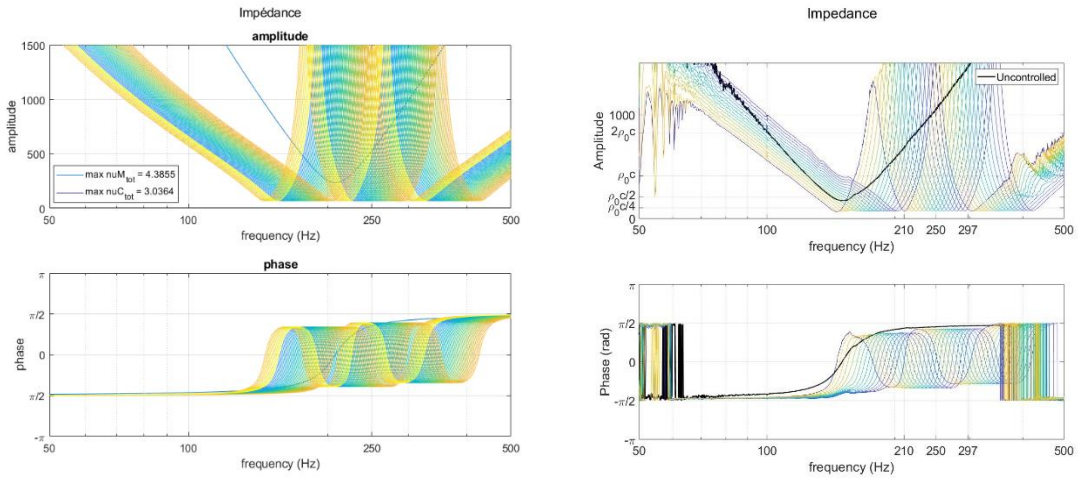

Figure 4.3: 3-DOF impedance target (left) and experimental realisation (right) for an array of speakers

The well-known Snell-Descartes Law of reflection, linking impinging angle and reflected angle by the simple formula $sin\Theta_i + sin\Theta_r = 0$ is valid if the interface where the reflection occurs, is planar and homogeneous. We can then define the reflection coefficient as a constant. However, if this reflection coefficient is space-dependent, the previous law has to be generalized, to take into account the phase gradient of the reflection coefficient. In the case of a 2D propagation with a varying reflection coefficient along axis x, we can define the Generalized Snell-Descartes Law (GDSL):

$$\sin\theta_i + \sin\theta_r = -\frac{1}{k}\frac{\partial\phi}{\partial x}, \qquad \text{with } k \text{ the wave number.}$$

However, in certain conditions of phase gradient and incident angle, this equation is no longer valid as the sine of the reflected angle is superior to 1. Therefore, the GDSL has to be corrected by taking into account the higher orders of reflection that we will not detail here. In fact, it can be shown that if the amplitude of the reflection coefficient is lower than one, the higher order of

reflection can be neglected. What happens then is a wave-conversion of airborne impinging waves to surface waves. These surface waves are rapidly absorbed if the amplitude of the reflection is, again, less than one.

With the multiple DOF introduced earlier, it is possible to apply the necessary phase gradient over a large frequency-band. Moreover, the impedances needed to achieve this phase-gradient are only dissipative. This kind of control is then purely stable, provided the model of the loudspeaker is perfectly known.

When applied in a duct, such a treatment would mitigate the propagation of sound. Simulation results can be seen on Figure 4.4**Error! Reference source not found.**.

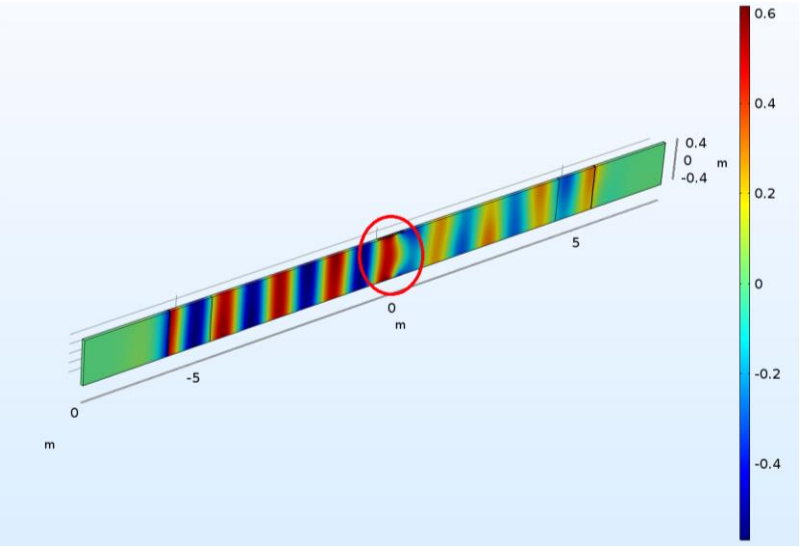

Figure 4.4: Insertion loss with a wave-conversion active liner (in the red circle)

4.2. The Distributed Impedance Control law– Stability Analysis

The Distributed Impedance Control Law proposed in 0 is an advection equation, linking the normal acceleration at the boundary to both the temporal and tangential derivative of pressure. The coupling between an acoustic domain inside a waveguide, and such transport boundary condition, is numerically analysed in 0. Thanks to the sectional duct mode study in an infinite waveguide, we demonstrate that the designed distributed impedance prevents plane wave to propagate in the positive x-direction, while allowing the plane waves propagating in the negative x-direction (see Figure 4.5). This confirms the acoustic diode (or isolator) effect, as already shown in 0 in the 1D approximation.

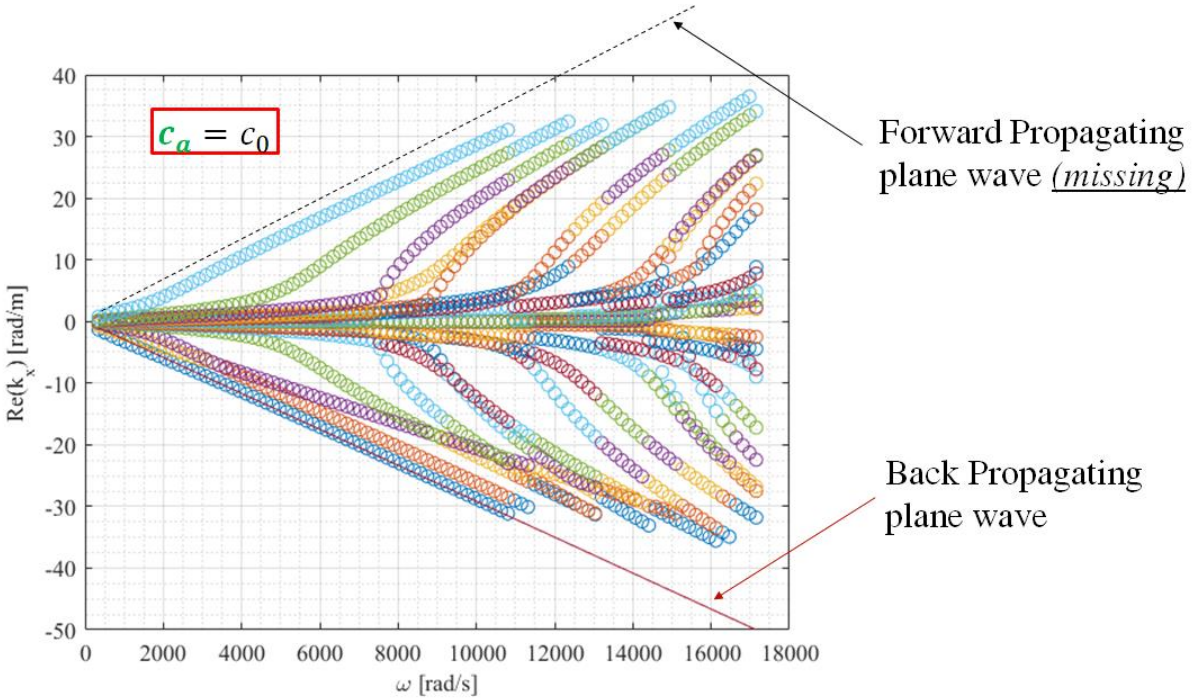

Figure 4.5: Dispersion Curves relative to the sectional duct modes into an infinite waveguide bounded on one side by the Distributed Impedance Law.

Based on the same analysis, it has been possible to assess the wave propagation stability criteria inside an infinite waveguide with a generalized non-local impedance boundary condition (see 0). The result is that our transport boundary condition will not bring unstable duct modes, if the celerity coefficient c_a is lower or equal than the sound speed in the medium c_0 (see Figure 4.6). Same result is attained for the time stability of the Cavity Modes in a finite acoustic waveguide (see **Figure 4.7**).

The implementation of the Distributed Impedance Control law through the electroacoustic resonators (the controlled loudspeakers), nevertheless, brings about new challenges both in terms of stability and robustness of the control. The distributed control law can indeed inject energy into the acoustic domain, which can easily break the stability if this energy is not damped by other passive systems.

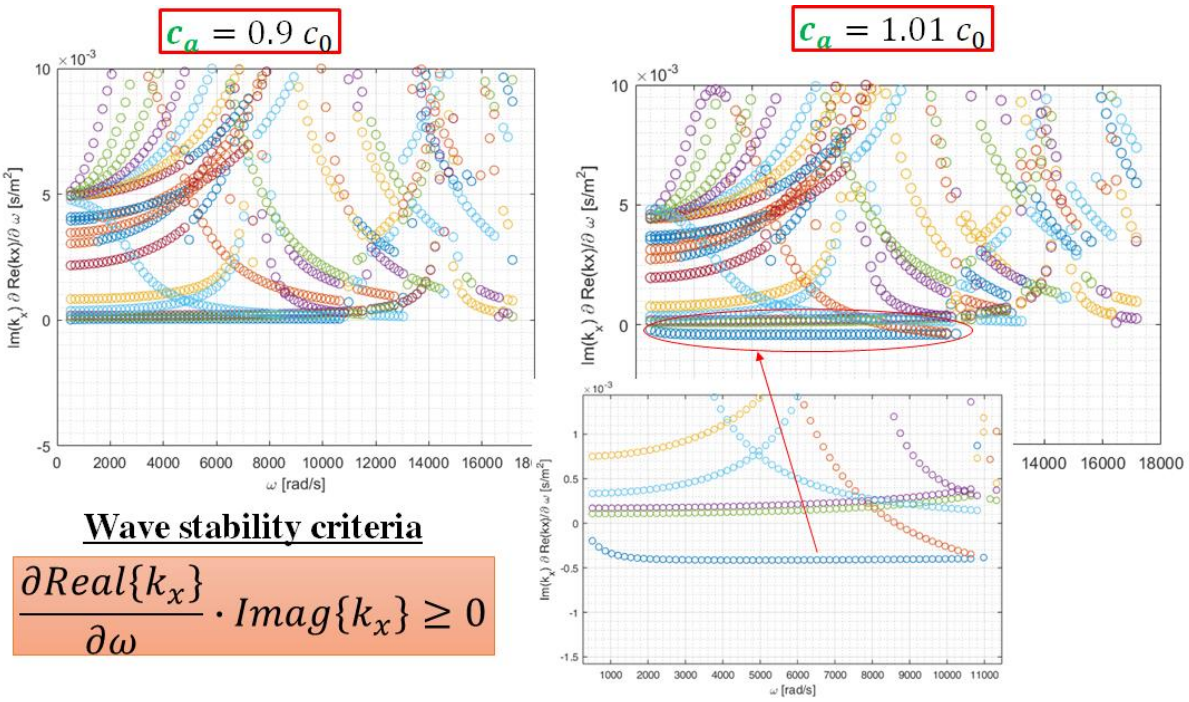

Figure 4.6: Wave Stability Criteria satisfied in the case of $c_a <= c_0$, but not in the case of $c_a > c_0$.

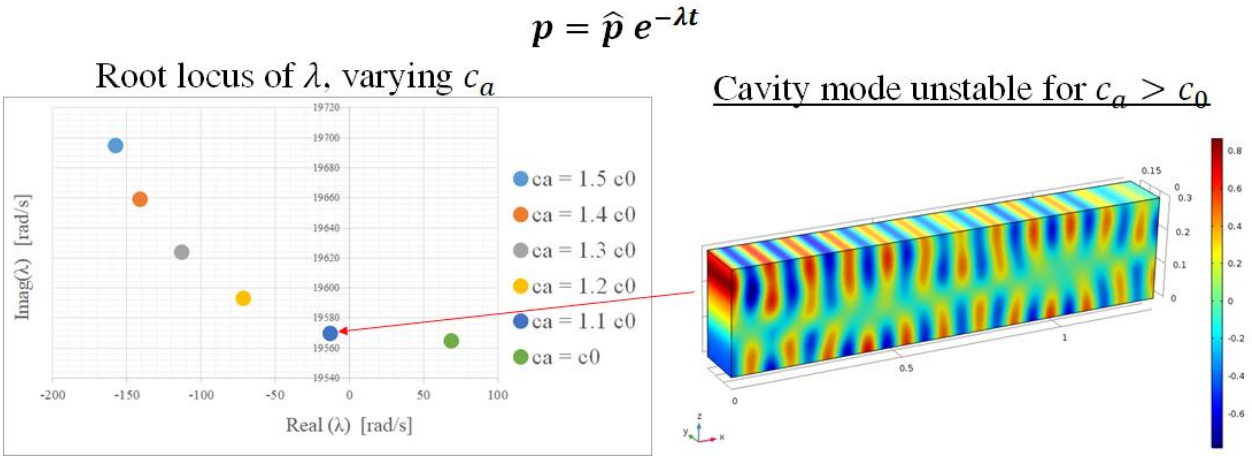

Figure 4.7: Time stability of the Cavity modes of a finite waveguide, bounded by the Distributed Impedance. The convention adopted is $p = \hat{p}\, e^{-\lambda t}$.

4.3. References

[4.1] R. Boulandet, H. Lissek, S. Karkar, M. Collet, G. Matten, M. Ouisse, M. Versaevel (2018). "Duct modes damping through an adjustable electroacoustic liner under grazing incidence. Journal of Sound and Vibration". *J. Sound and Vibration* 426. 19 - 33. 10.1016 (2018).

[4.2] M. Collet, P. David, and M. Berthillier. "Active acoustical impedance using distributed electrodynamical transducers". *J. Acoust. Soc. Am.*, 125(2), (2009).

[4.3] E. De Bono, M. Collet, S. Karkar, "Analysis of a transport equation as a boundary condition in an acoustic transmission line", *ISMA 2018 conference (2018).*

[4.4] S. Karkar, M. Collet, "Nonreciprocal Acoustics Using Programmable Boundary Conditions: From Boundary Control and Active Metamaterials to the Acoustic Diode". *ASME. Smart Materials, Adaptive Structures and Intelligent Systems, Vol. 2* (2017).

[4.5] E. Rivet, "Room Modal Equalisation with Electroacoustic Absorbers", *Thesis, EPFL*.(2016)

5. Aerodynamic Noise Reduction by Porous Materials (ESR7)Introduction

ESR7 has been focusing on elucidating the working principle of porous materials for reducing aerodynamic noise, particularly in the case of edge noise [5.1-5.5] (e.g., leading edge and trailing edge noise). A recent experimental study by Rubio-Carpio et al. 0 have shown that replacing the trailing edge of an airfoil with metal-foam resulted in noise reduction at low to mid frequency ranges. The authors concluded that the noise reduction mechanism is likely to be linked with the unsteady transpiration across the porous material, since non-permeable porous trailing edge did not result in noise reduction. They have also pointed out some changes in the flow-field due to the use of porous material, however no clear conclusion was drawn. It was speculated that the noise reduction might be due to the different surface impedance between the porous and the solid trailing edges. Furthermore, it is also hypothesized that the acoustic scattering mechanism by the porous trailing edge might be different from the solid. However, due to the limitations of the experimental technique, they were not able to observe the flow field in proximity of the porous material surface. Some forms of measurement such as surface pressure is also unfeasible to perform. Therefore, numerical simulations may complement the data obtained from the experiments. Nonetheless, this will require accurate numerical representation of the physical properties of porous material.

5.1. Validation Study of Porous Material Model in PowerFLOW

The first step in this study would be to validate the numerical model of the porous material in the lattice-Boltzmann solver PowerFLOW. One of the widely-known model, the Hazen-Dupuit-Darcy 0 (HDD), describes the momentum loss of a flow field permeating through a porous material. The model characterizes the porous material with two parameters, namely the permeability (K) and the form coefficient(C), which are mathematically expressed as follow.

$$\frac{\Delta P}{h} = \frac{\mu}{K} v_d + \rho C v_d^2$$

where ρ is the fluid density, μ is the dynamic viscosity, $v_d = Q/A$ is the Darcian velocity, Q is the volumetric flow rate, A the cross-section area of the sample, and h is the material thickness. PowerFLOW uses slightly different nomenclature to describe the HDD parameters, namely the viscous resistivity ($R_V = \mu/K$) and inertial resistivity ($R_I = C$). Furthermore, there are two different models of porous media in PowerFLOW – APM (acoustics porous medium) and PM (porous medium). While both describes the porous material as an equivalent fluid region governed by the HDD model, the APM also considers acoustic absorption property of the material. Additionally, APM is assigned with a porosity (Φ) value which would affect the flow behavior at the interface in between the regular fluid region and the APM region.

Table 5.1 Parameters of the metal foam sample

d_c (μm)	Φ (%)	R_V (Ns/m^4)	R_I (m^{-1})
450	89.28	29850	9758
800	91.65	6728	2613

The validation case is the porous material test rig that has been used by Rubio-Carpio et al. 0 to characterize the metal foam properties (Figure 5.8). The porous material that will be used is based on a NiCrAl metal-foam manufactured by *Alantum*. The manufacturer specified the metal-foam characteristics with mean cell diameter d_c . The porous material parameters are summarized in Table 5.1. The resistivity of the metal foam would depend on the thickness of the sample, hence it would be quite challenging to numerically model a porous material sample of arbitrary shape. To overcome this issue, the metal-foam sample is modeled as 3-layer of acoustics porous material (APM) - porous material (PM) - APM. The APM region accounts for 20% of h (i.e., 0.1h thick on both ends of the sample) and the rest of the thickness is prescribed as PM region. A mass flow corresponding to certain Darcian velocity (v_d) is allowed inside the tube, and the resulting pressure drop caused by the metal foam sample is measured.

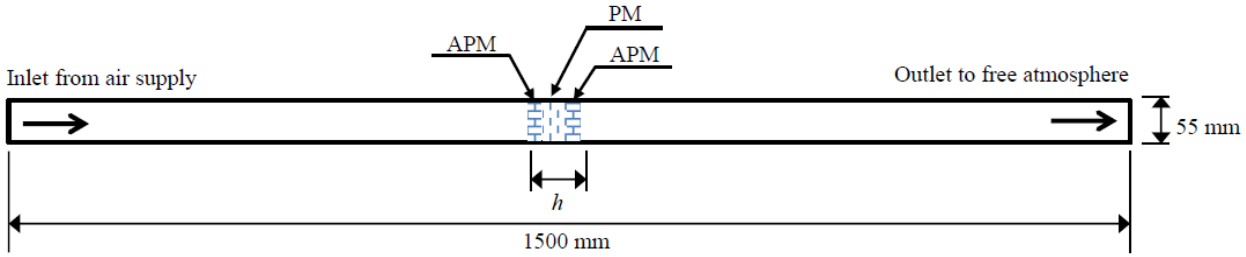

Figure 5.8: Simplified sketch of the test rig for characterizing the permeability and the form coefficient of the metal-foam sample

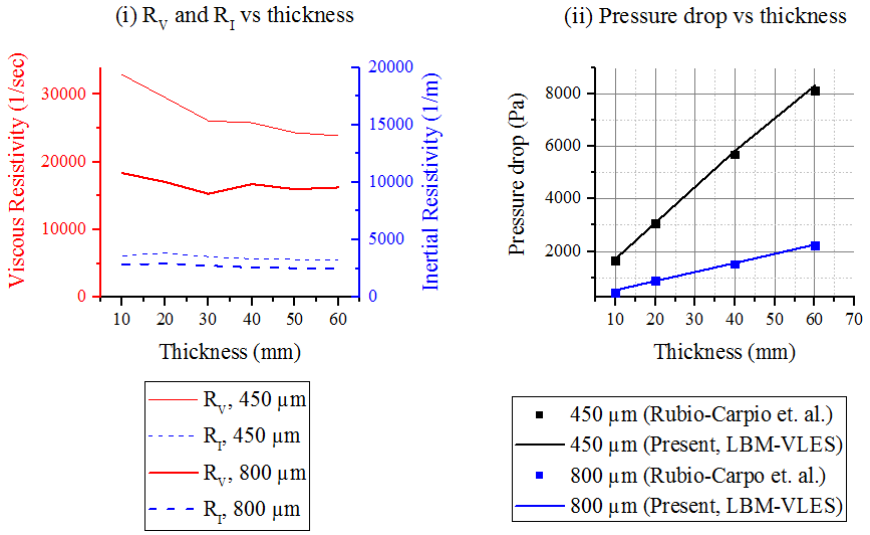

Figure 5.9: Resistivity value and pressure drop variation with metal-foam sample thickness in the test rig

The variation of viscous resistivity R_V , inertial resistivity, R_I, and the pressure drop trend in the porous material characterization test rig is shown in Figure 5.9. The resistivity values were extracted from measurements of Rubio-Carpio et al. 0, which is then provided into PowerFLOW. Figure 5.9 (ii) shows that the APM-PM combination used in the numerical study results in good agreement for various tested sample thickness.

5.2. Preliminary Conclusion and Outlook

The porous material model in PowerFLOW has been shown to produce accurate pressure drop trend. However, more validation studies will be performed on more realistic cases, such as the trailing edge noise case of Rubio-Carpio et al. 0. Some interesting concepts, such as a combination of porous material and trailing edge serration 0, may be introduced to obtain even greater noise reduction.

5.3. References

[5.1] Roger, M., Schram, C., & De Santana, L., "Reduction of airfoil turbulence-impingement noise by means of leading-edge serrations and/or porous material." *19th AIAA/CEAS aeroacoustics conference*, p. 2108, 2013.

[5.2] Geyer, T., Sarradj, E., & Fritzsche, C., "Measurement of the noise generation at the trailing edge of porous airfoils." *Experiments in Fluids*, Vol. 48, No. 2, 291-308, 2010

[5.3] Carpio, A. R., Martínez, R. M., Avallone, F., Ragni, D., Snellen, M., and Van Der Zwaag, S., "Broadband Trailing Edge Noise Reduction Using Permeable Metal Foams." In *46th International Congress and Exposition of Noise Control Engineering*, p. 27-30, August 2017.

[5.4] Khorrami, M. R., & Choudhari, M. M. "Application of passive porous treatment to slat trailing edge noise." *NASA Technical Report*, NASA-TM-2003-212416, 2003.

[5.5]Sarradj, E., & Geyer, T. "Noise generation by porous airfoils." *13th AIAA/CEAS Aeroacoustics Conference Proceedings*, No. 3719, May 2007.

6. Efficient numerical modelling of advanced liners (ESR-14)

The most common noise mitigation strategy consists in the installation of acoustic liners, which properties are optimized for the given geometrical set-up and source configuration. Existing numerical techniques dealing with the optimization of the liner parameters (depth, resistance, reactance, etc.) are computationally very intensive. The main goal of this research is to investigate novel domain decomposition techniques to reduce the computational cost associated with the liner optimization process.

Domain decomposition methods, which consist in solving a boundary value problem by splitting it into smaller boundary value problems on subdomains and iterating to coordinate the solution between adjacent subdomains, are often used to parallelize the solution of large scale acoustic problems. Two different non-overlapping domain decomposition algorithms namely FETI-H [6.1] and FETI-2LM [6.2] were first implemented and compared for the modelling of acoustic problems in the presence of bulk-reacting acoustic liners. The latter are modelled using the so-called equivalent fluid approach, in which the propagation is described using the Helmholtz equation with equivalent, complex-valued density and equivalent bulk modulus [6.3]. It was found that in the absence of a global coarse space preconditioner the FETI-2LM outperforms FETI-H for higher wave-numbers and large number of partitions. However, FETI-H requires half the interface problem size and thus provides desirable gains on the Gram-Schmidt orthogonalization process. In order to apply this technique in an optimization framework, the FETI-2LM version is chosen.

The FETI-2LM method was first applied to Helmholtz problem by De La Bourdonnaye et. Al [6.2] which introduces 2 Lagrange multipliers or the “dual” variables on the inter- faces of the partitioned subdomains. This method has been implemented and validated on a simple duct-liner configuration.

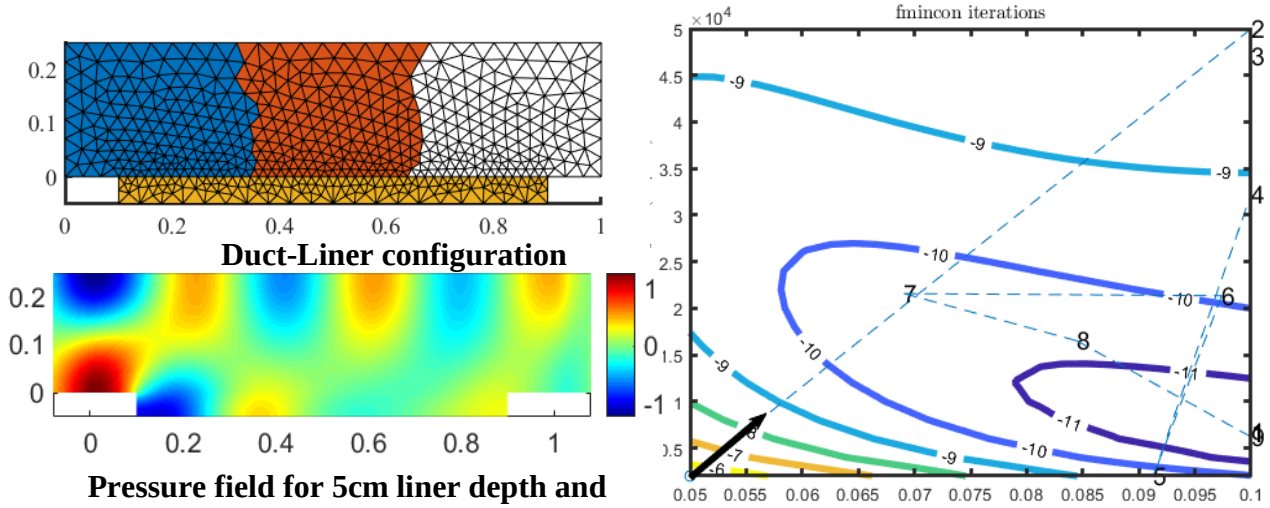

Figure 6.10 fmincon optimization results for first mode, 1kHz using an initial guess (5cm, 2e3 Ns/m^4) = 11.77 dB

allows to easily modify the liner properties at a frequency without modifying the partitioning inside the duct. This in turn enables storing the in-duct partitions LU factors once, thus avoiding the cost of having to repeatedly re-assemble and re-factorize them at each optimization step. In this analysis, the one parameter Miki model is chosen to estimate the equivalent fluid properties in the liner. The flow resistivity and the liner depth are chosen as the critical parameters which need to be optimized. Figure 6.10 shows the optimization performed for a duct liner test case using 3 duct partitions for the first cut-on mode at 1kHz. The local gradient-based optimizer "fmincon" from Matlab [6.4] is used to demonstrate this new improved workflow. Let us now examine the computational cost savings induced by the proposed strategy.

The three main computationally intensive tasks in the method are the initial factorization of the local subdomain matrices, the successive forward-backward substitutions to solve the local problems and the modified Gram-Schmidt orthogonalization [6.5]. The first task requires a significant computational effort, although this cost is independent of the number of iterations to converge. Reusing the stored LU factors at a particular frequency for all optimization steps minimizes this cost drastically.

However, the cost for the latter two tasks is highly dependent on the number of iterations required for the convergence of the interface problem. In the case when only one partition is chosen in the liner, this cost can be reduced by recycling the Krylov subspace based on the GCRO-DR (Deflated Restarting) method [6.6]. By using the same initial guess as obtained from the previous optimization evaluation in the GCRO-DR method, preliminary results showed a promising 40-60% cost reduction on the number of iterations.

The proposed workflow, combining domain decomposition methods and Krylov subspace recycling strategies, allows to drastically reduce the computational costs associated with the optimization of a bulk-reacting liner. This strategy can allow us to perform more optimizations, and in turn to design more efficient non-local acoustic liner concepts. The next steps will include extending this workflow to include mean flow effects and applying it on realistic liner test cases.

6.1. References

[6.1] A. M. M. L. F.-X. R. e. a. Charbel Farhat, «Two-level domain decomposition methods with Lagrange multipliers for the fast iterative solution of acoustic scattering problems,» *Computer methods in applied mechanics and engineering*, vol. 184, pp. 213-239, 2000.

[6.2] C. F. A. M. F. M. a. F. R. A. de La Bourdonnaye, «A nonoverlapping domain decomposition method for the exterior Helmholtz problem,» *Contemporary Mathematics*, pp. 218:42-66, 1998.

[6.3] M. Y., «Acoustical properties of porous materials - Modifications of Delany-Bazley models,» *The Journal of the Acoustical Society of Japan*, vol. 11(1), pp. 19-24, 1990.

[6.4] N. The MathWorks, *Matlab Optimization Toolbox, 2018a*, MA, USA, 2018.

[6.5] F. R. a. A. Barka, «Block Krylov Recycling Algorithms for FETI-2LM Applied to 3-D Electromagnetic Wave Scattering and Radiation,» *IEEE Transactions on Antennas and Propagation*, pp. 65:1886-1895, 2017.

[6.6] E. D. S. G. M. D. D. J. MICHAEL L. PARKS, «RECYCLING KRYLOV SUBSPACES FOR SEQUENCES OF,» *Society for Industrial and Applied Mathematics*, vol. 28, pp. 1651-1674, 2006.

7. Summary

This report gives an overview of progress regarding acoustic attenuation techniques from the work of five fellows in the SmartAnswer ITN-project. These fellows are about one and a half year into their PhD-studies. The results obtained so far can be summarized as:

ESR3 has initiated a study on high acoustic excitation level harmonic interaction effects on the acoustic properties of perforates. This is relevant for optimizing noise control solutions for applications such as: gas-turbines, aircraft engines and automotive mufflers where perforates are used for noise control purposes and exposed to high acoustic excitation levels.

ESR4 is focusing on the aeroacoustics behavior of materials including flow acoustics interaction. The first investigated material was a corrugated surface used in industrial pipes. A micro-perforated liner composed of honeycomb Helmholtz resonators, such as used for aircraft engine applications, has also been studied. The liner has been used to test the accuracy of numerical multimodal methods by comparison with experimental data.

ESR5 is studying the concept of adaptive methods to obtain noise control by changing the impedance of an electroacoustic absorber. Control strategies include: Local Impedance Control, as well as Non-Local (or Distributed) Impedance Control using a programmable Digital Signal Processor, which controls the current inside the loudspeaker to vary its membrane velocity. The control output is based upon the measured acoustic pressure in the vicinity of the loudspeaker membrane. In this way a desired impedance, to produce noise control, could be reproduced.

ESR7 has been focusing on elucidating the working principle of porous materials for reducing aerodynamic noise, particularly in the case of edge noise (e.g., leading edge and trailing edge noise for airfoils). Both experimental work and numerical simulations using PowerFLOW has been part of the study. Further studies will include concepts, such as a combination of porous material and trailing edge serration to potentially obtain even greater noise reduction.

ESR14 is studying numerical techniques for simulating and optimizing the noise reduction of acoustic liners.The main goal of this research is to investigate novel domain decomposition techniques to reduce the computational cost associated with the liner optimization process